Journal of Materials Chemistry A

Accepted Manuscript

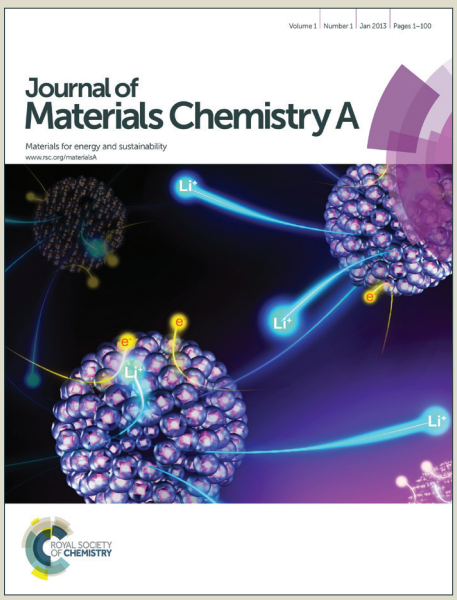

ROYAL SOCIETY OF CHEMISTRY

www.rsc.org/materialsA

Table of Contents (TOC)

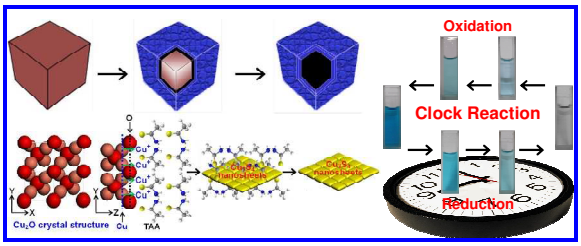

Ultrathin Cu_7S_4 nanosheets constructed nanocages were one-step synthesized based on Kirkendall Effect, which could effectively catalyze the 'clock reaction' of methylene blue.

Journal Name RSCPublishing

ARTICLE

Ultrathin Cu_7S_4 Nanosheets Constructed Hierarchical Hollow Cubic Cages: One-step Synthesis Based on Kirkendall Effect and Catalysis Property

Cite this: DOI: 10.1039/x0xx00000x

Received 00th January 2012,
Accepted 00th January 2012

DOI: 10.1039/x0xx00000x

www.rsc.org/

Yingchang Jiang,[ab]† Shudong Zhang,[a]† Qi Ji,[c] Jian Zhang,[a] Zhongping Zhang,*[a] and Zhenyang Wang *[a]

Ultrathin two-dimensional (2D) nanosheets are a conceptually new category of nanoscale materials. Integration/assembly of individual 2D nanosheets into 3D hierarchical structures is an enormous challenge and an essential requirement for the application. Here we first report the direct synthesis of Cu_7S_4 hierarchical hollow cubic cages assembled by ultrathin nanosheets based on Kirkendall Effect. Slowly released Cu^+ from Cu_2O cubic template-crystals and S^{2-} from decomposed thioacetamide (TAA) can react with each other and form a diffusion pair, which provides a thermodynamic and kinetic equilibrium to be responsible for formation of the ultrathin Cu_7S_4 nanosheets and the Cu_7S_4 hierarchical hollow cubic cages. Using this unique hollow structure and the outstanding catalyzed property of Cu_7S_4 nanosheets, as an example, we successfully demonstrate that Cu_7S_4 nanocages can effectively catalyse the "clock reaction", which is a periodic cycle redox oscillation reaction between methylene blue (MB) and colorless leuco methylene blue (LMB). The unique hierarchical structure has been found to enhance the rate of this redox reaction via the ultrathin nanocatalyst. This work develops a facile strategy for synthesizing 3D hierarchical structures constructed by atomically thick single layers and demonstrates their superior ability to optimize nanosheet-catalyzed clock reaction.

Introduction

Two-dimensional (2D) nanosheets have focused on tremendous attention because of their promising practical applications and theoretical values.[1-7] The ultrathin nanosheets are able to not only enhance the intrinsic properties of their bulk counterparts but also generate new promising properties.[8] To date, with the emergence of graphene, more attention has been attracted on the inorganic graphene analogues (IGAs) with weak vander Waals forces among the layers, which can be easily exfoliated into 2D nanosheets with atomic thickness, such as single layered transition-metal dichalcogenide nanosheets,[8,9] and ultrathin g-C_3N_4 nanosheets,[8a] and so on. Recently, ultrathin nanosheets have been fabricated by anisotropic growth,[8a] the developed liquid exfoliation strategy,[8e, 10] electrochemical lithiation-exfoliation process[9e], mechanical cleavage[9c, 11], or CVD growth[12, 13]. These individual 2D nanosheets are the most promising building blocks for integration into other macroscopic 2D materials such as polymers and self-assembly into various macroscopic structures, such as paper-like materials[14], flexible transparent and conductive films.[15, 16] Vacuum-filtration assembly and Langmuir–Blodgett (LB) technique have been commonly applied for the preparation of various free-standing macroscopic 2D structural films/papers. Although macroscopic paper-like materials and films have been successfully assembled by ultrathin 2D nanosheets, fabrication or integration of other individual 2D nanosheets into 3D hierarchical structures still lack an effective method and remain a great challenge.

Recently, three-dimensional foam-like graphene macrostructures,[17] called graphene foams (GFs), have been directly synthetized by template-directed chemical vapor deposition and controllable self-assembly method[18-20]. And the GFs consist of an interconnected flexible network of graphene as the fast transport channel of charge carriers for high electrical conductivity. The electrical conductivity of GFs is higher than a series of graphene-based composites[21-23] and macroscopic structures[14-16, 24]. Therefore, fabricating or integrating other individual 2D nanosheets into 3D hierarchical structures will spark new scientific interest and practical applications.

Copper sulfide, a non-stoichiometric p-type semiconductor (band gap 1.2–2.0 eV), exhibits great potential for wide applications in solar cells, nanoswitches, thermoelectric and photoelectric transformers, and photocatalytic performances[25-27]. Many works have been reported on the synthesis of copper sulfide nanocages through a sacrificial Cu_2O template approach based on the Kirkendall effect.[28] Although various Cu_7S_4 cages with single-crystalline shells (such as cubes, octahedra, and 18-facet polyhedra)[27b, 28], polycrystalline (such as cubes, and 26-facet polyhedra) and meso-crystalline shells[26, 27] have been successfully synthesized by using single-crystalline Cu_2O

Journal Name RSCPublishing

ARTICLE

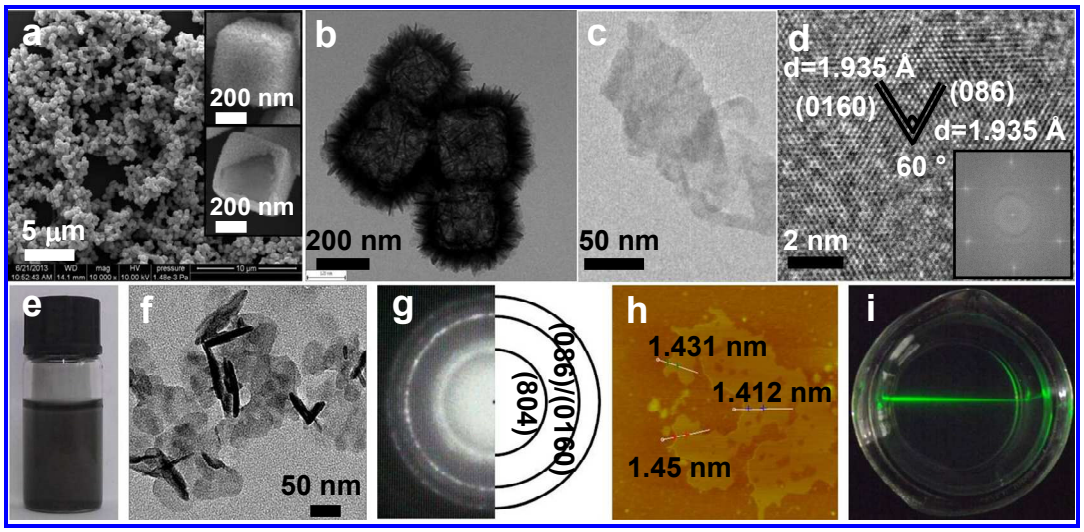

Fig. 1 Overview SEM (a) and TEM (b) image of Cu_7S_4 hierarchical hollow cubic cages. (c) TEM image of a typical Cu_7S_4 ultrathin nanosheet. (d) HRTEM image of a typical Cu_7S_4 nanosheet (inset, an FT pattern corresponding to the HRTEM image). (e) TEM image of Cu_7S_4 ultrathin nanosheets. (g) SAED pattern of Cu_7S_4 ultrathin nanosheets. (h) Tapping-mode AFM image of Cu_7S_4 ultrathin nanosheets. (i) Tyndall effect of the synthetic ultrathin nanosheets dispersed in water.

crystals as sacrificial templates. Therefore, the preparation of new classes of Cu_7S_4 structures with high complexity is not only important for a wide range of applications but also significant for developing modern synthetic methodologies. Herein, we report on the large-scale synthesis of 3D Cu_7S_4 hierarchical hollow cubic cages assembled by ultrathin nanosheets based on Kirkendall Effect, which was supported by a detail time-dependent morphology evolution study. The X-ray diffraction (XRD) pattern clearly shows that the monoclinic Cu_7S_4 (with lattice constants of a = 53.79 Å, b = 30.90 Å, c = 13.36 Å, and β = 90°, JPCDS No. 23-0958) structure could be indexed for products obtained by Kirkendall Effect under the room temperature (Fig. S1a, ESI). Energy-dispersive spectroscopy (EDS) analysis of the synthetic Cu_7S_4 cubic cages shows that the obtained products are mainly composed of Cu and S without any impurity, with a Cu/S molar ratio of ~1.749:1 (Fig. S1b, ESI), which is close to the stoichiometric ratio of Cu_7S_4.

Results and discussion

Structural characterization

The typical SEM image, as shown in Fig. 1a, gives a panoramic picture of the product, which reveals that it is completely composed of Cu_7S_4 hierarchical cubic micro-/nano-structures with an average length of ~400 nm. Moreover, careful observation on a typical cubic architecture (upper inset of Fig. 1a) can find that it is assembled by very thin nanosheets. Interesting, the interior space of the hollow Cu_7S_4 cubic cages is clearly revealed on the individual broken cubic cage FESEM image (bottom insert of Fig. 1a). And hollow interior can simultaneously be observed by transmission electron microscopy (TEM) (Fig. 1b). For more information about Cu_7S_4 nanosheets, hollow Cu_7S_4 cubic cages were sonicated to obtain free-floating Cu_7S_4 nanosheets, which are ~100 nm in size (Fig. 1c and 1f). The representative high-resolution TEM image corresponding fast Fourier transform (FT) pattern in Fig. 1d clearly shows the crystalline structure of a Cu_7S_4 nanosheet. The continuous lattice fringes demonstrate the single-crystal nature of the nanosheet, the lattice spacings of 0.1935 nm correspond to (086) and (0160) lattice planes, respectively. The obtained Cu_7S_4 nanosheets are preferentially exposed {100} surface. The corresponding electron diffraction (ED) pattern image (Fig. 1g) also indicates the high quality of the Cu_7S_4 crystals. The thickness of the as-obtained Cu_7S_4 nanosheets was measured by tapping-mode atomic force microscopy (AFM) (Fig. 1h). It is amazing that the thickness of a single layer of the synthetic nanosheet is only ~ 1.43 nm, which is comparable to the thickness of graphene oxide. The well-defined Tyndall effect of a transparent solution of ultrathin Cu_7S_4 nanosheets (Fig. 1i) indicates the presence of highly monodisperse ultrathin nanosheets in ethanol. The suspension was very stable, and no aggregation was observed upon standing for more than one month. Furthermore, the optical band gap of Cu_7S_4 nanocages was investigated by UV-vis spectroscopy (Fig. S2, ESI). For a crystalline semiconductor, the optical absorption near the band edge follows the equation $\alpha h\nu = A(h\nu - E_g)^n$, where α, ν, E_g and A are the absorption coefficient, the light frequency, the band gap, and a constant, respectively. The estimate value of E_{photon} at α = 0 shows an absorption edge energy corresponding to E_g = 2.58 eV for Cu_7S_4 cages assembled by ultrathin nanosheets and 2.48 eV for Cu_7S_4 cages assembled by ~20 nm nanoplates. Compared with the values of 2 eV for bulk counterpart[29], it can

be observed that a larger blue shift absorption profile has occurred, which might be attributed to the quantum size effects considering the introduction of nanotwinned nanosheets building blocks into the shells of the hollow architectures.[26]

Formation mechanism

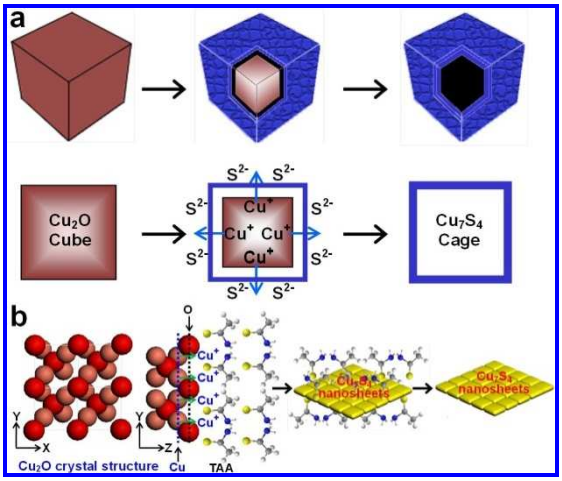

Fig. 2 Schematic illustration of the structure evolution of a Cu_7S_4 hollow nanocubic structure (a) and Cu_7S_4 ultrathin nanosheets growth (b).

The mechanisms of Cu_7S_4 hollow nanocubic structure formation and Cu_7S_4 ultrathin nanosheets growth were proposed and further demonstrated by monitoring the intermediate products and turning the experimental conditions (Fig. 2). While the formation of Cu_7S_4 ultrathin nanosheets mainly lies on the growth rate of Cu_7S_4, the key point in our synthesis of Cu_7S_4 hierarchical hollow cubic cages involves a self-sacrificing template process, which is slowly released Cu^+ from Cu_2O cubic template-crystals and S^{2-} slowly decomposed from thioacetamide (TAA) upon a room temperature hydrolysis (Fig. 2a). In our approach, as the reaction proceed, the diameters of the cubic solid Cu_2O (Fig. S3, ESI) inner cores become smaller and smaller, with the accompaniment of increasing crystallization of Cu_7S_4 ultrathin nanosheets, confirming the occurrence of a Kirkendall-effect-induced hollowing process (Fig. S3, ESI). The final hollow cubic nanocages in this reaction have been confirmed to be Cu_7S_4 on the basis of the corresponding XRD patterns. The intermediate products were collected at different stages, and their morphologies and structural informations were subjected to SEM and XRD investigations (Fig. S4, ESI), respectively. And the different experimental conditions further verify that the conversion process was from Cu_2O to Cu_7S_4 in an air atmosphere (Fig. S5, ESI). Detail experiments reveal that S^{2-} and Cu^+ anion-cation ions release rate leads to the formation of Cu_7S_4 ultrathin nanosheets. TAAs slowly decompose and produce low concentration S^{2-} at room temperature (TAA decomposition rate was tested in Fig. S6a, ESI). On the other hand, the undecomposed TAA can stabilize the Cu_7S_4 ultrathin nanosheets by reducing the diffusion rate of S^{2-} into the surface of Cu_7S_4 ultrathin nanosheets, as drawn in Fig. 2b. Such an interaction between TAA and Cu_7S_4 crystals can also be confirmed by the FTIR spectroscopic analysis (Fig. S6b, ESI). The C=S stretching band of TAA appears in the products without washing with distilled water and ethanol, indicating that TAA adsorb on the surfaces of the Cu_7S_4 crystals. The interaction between TAA and Cu_7S_4 crystals has also been verified by the shift of C=S stretching band of TAA from ~1028 cm^{-1} originally (Fig. S6b(a), ESI) to a lower frequency of ~1017 cm^{-1} (Fig. S6b(b), ESI) in the FTIR spectra. But, the C=S and other functional group signals (Fig. S6b(c), ESI) do not arise from the absorbed TAAs on the surface of the final product, which is removed ever by washing with distilled water and ethanol several times. Meanwhile, when TAA was replaced with Na_2S, Cu_7S_4 nanoplates with thickness of ~20 nm were obtained (Fig. S7a, ESI). And Cu_7S_4 particles around the external surfaces of the Cu_2O crystals were produced using thioure (dissociation temperature more than 80 °C) under the same reaction condition (Fig. S7b, ESI). Those results suggest the crucial role of release rate of S^{2-} from TAA. More experimental observations, which have been performed to confirm the critical impact of release rate of S^{2-} from TAA, including the effect of temperature (Fig. S8, ESI) detailed in the Supporting Information of this report.

Catalysis of Clock Reaction:

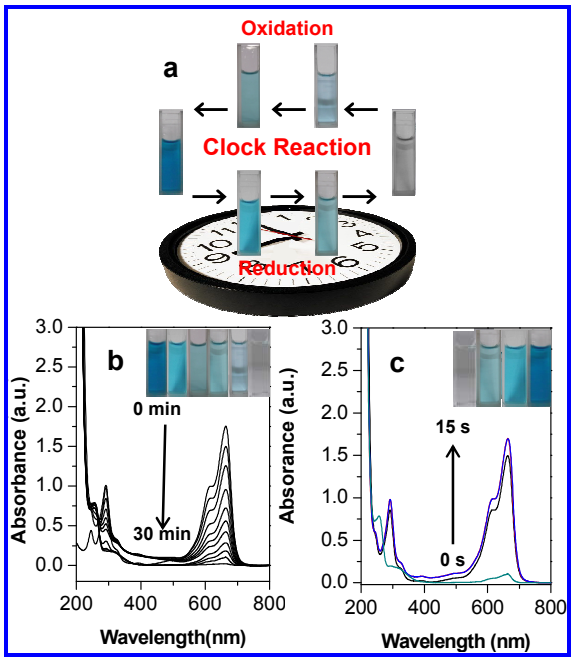

Fig. 3 (a) Schematic representation of the "clock reaction", that is, blue color fading and regeneration of MB. Absorption spectra for successive decolorization of MB (b) and colour regeneration (c).

As well known, the nano-scale copper compounds have very good catalytic performance.[30, 31] To study the catalytic properties of the Cu_7S_4 nanocages constructed by ultrathin nanosheets, we demonstrated its catalytic action for methylene blue (MB)–hydrazine reaction in aqueous medium. An oscillation between blue color MB and colorless leuco methylene blue (LMB) solution was observed on periodic shaking. The process of redox reaction demonstrates a simple "clock reaction", which provides an engaging illustration of redox phenomena, reaction kinetics, and the principles of chemical titration, as shown in Fig. 3a. Based on MB exhibiting an intense absorption band in the region 200-800 nm[32] and

LMB no absorption (Fig. S9, ESI), we monitored the process of the clock reaction by a UV-visible spectrophotometer in the mixed solution of MB and ultrathin Cu_7S_4 nanosheet constructed nanocages. Then the MB blue color bleaching starts, a steady decrease of the absorbance of MB was measured at same intervals, as shown in Fig. 3b. In the absence of Cu_7S_4 nanocages, no such a decrease in absorbance of MB was observed in the same experimental condition. Meanwhile, other copper compounds, such as CuO and Cu nanoparticles, could not exhibit the "clock reaction".[30] Thus, the important role of Cu_7S_4 ultrathin nanosheets and nanocages in the "clock reaction" is no doubt established. In fact, Cu_7S_4 nanocage catalysts have a strong catalytic ability for the reduction of methylene blue at room temperature. After complete reduction of MB, the solution contains colourless LMB which again regenerates the blue colour in the presence of small amount aerial O_2 on shaking of the reaction mixture as shown in Fig. 3c. Under the catalysis of the ultrathin Cu_7S_4 nanosheets catalyst, the plot of absorption factor as a function of time (Fig. S10a, ESI) shows a profile of exponential equation, $[A]=[A]_0e^{-kt}$, which is consistent with a pseudo-first-order reaction. Moreover, according to the first-order reaction, a plot of lnA_t *vs time* (Fig. S10b, ESI) shows a linear relationship. This observation further confirms a pseudo-first-order reaction kinetics, and from the slope of this curve, rate constant value k was obtained. Interestingly enough, a plot of rate *vs* concentration of hydrazine gives a straight line (Fig. S10c, ESI). All above results also support the pseudo-first-order kinetics. However, no Cu_7S_4 cages catalyst, no catalytic reaction happens. The catalytic reaction was monitored at different temperatures, and by using the Arrhenious equation $lnk_2/k_1=E_a/R(T_2-T_1)/T_2T_1$, the activation energy (E_a) of the reduction of MB is calculated to be 3.358 kJ mol^{-1} (Fig. S9d, ESI). This result reveals that the activation energy (*Ea*) of the reduction of MB reduced by 0.352 kJ mol^{-1} under the effect of the Cu_7S_4 nanocage catalyst, thereby making the reaction rate faster compared to the Cu_2O nanocube catalysts (E_a = 3.71 kJ mol^{-1})[30].

In order to evaluate the redox properties of the Cu_7S_4 nanocages constructred by nanosheets with the different thicknesses, the cyclic voltammetric (CV) response was investigated (Fig. S11, ESI). CV characteristic curve shows that Cu_7S_4 nanocages constructed by the ultrathin nanosheets with with the thickness of ~ 1.43 nm have lower oxidation potential and easier electrooxidation activity, comparing with Cu_7S_4 nanocages constructed by the ultrathin nanosheets with with the thickness of ~ 20 nm. Therefore, the electron transfer from hydrazine to MB fast takes place via Cu_7S_4 nanosheets surfaces because of the reasonable affinity of both the reductant (hydrazine) and oxidant (MB) to the high activity ultrathin nanosheet surfaces (Fig. 4a). The effect of catalyst dose on the reduction reaction is monitored by adding different amounts of catalyst in the reaction mixture under keeping the same condition. Here clock reaction was studied with different catalyst dosages. In all the cases with variable amounts of catalyst the plot of $ln(A/A_0)$ *vs Time* (min) (Fig. 4b) indicates the clock reaction ratio become faster with the catalyst dosage increasing. The percent conversion from MB to LMB of our designed hierarchical hollow cubic cages is up to 92% in 5 min (300 μL, ~1×10^{-5} M), over 5 times faster than that of other catalyst dosage (50 μL, ~1×10^{-5} M, 25 min) (Fig. 4b). Therefore, the catalytic performance may be ascribed to the hollow structures. More chemicals (ions) can be stored in the hollow structures of the sample with a greater chance of participating in the reactions, thus greatly improving the catalytic efficiency of the obtained nanostructures.

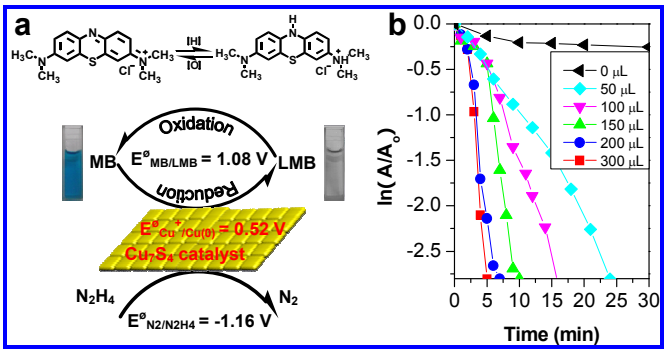

Fig. 4 (a) Scheme to show the catalytic activity of Cu_7S_4 ultrathin nanosheets for the clock reaction. (b) Plot of $ln(A/A_0)$ *vs Time* by varying the dose of the catalyst.

Conclusions

In conclusion, ultrathin 2D nanosheets assembling into Cu_7S_4 3D hierarchical hollow cubic cages have been successfully synthesized via a simple Kirkendall Effect. Furthermore, the widening of the band gap was observed as a result of the quantum confinement effects and structural factors, which will be useful in the energy band engineering. The electrochemical studies indicate that Cu_7S_4 nanosheets show lower oxidation potential and easier electrooxidation activity. The ultrathin Cu_7S_4 nanosheet-catalyzed clock reaction has been demonstrated using MB and hydrazine in an aqueous medium. This study is a base for developing integration of individual 2D nanosheets into 3D hierarchical new structures for wide applications in near future.

Experimental methods

All the reagents were of AR grade and were used without further purification. Double distilled water (18.2 MΩ) was used throughout the course of the reaction. $CuSO_4$, glucose, PVP (K-30), NaOH, Ascorbic acid, hydrazine hydrate, and methylene blue were purchased from Sinopharm Chemical Reagent.

1.1 Synthesis of Solid Cu_2O Cube Template Crystals.

Solid Cu_2O cubes were synthesized according to the reported method with minor modifications.[28b] Briefly, 0.20 g of PVP (polyvinylpyrrolidone) (K-30) was dissolved into 100 mL of $CuSO_4$ (0.01 M) aqueous solution under magnetic stirring at room temperature, followed by the addition of 25 mL of 1.50 M NaOH aqueous solution. Upon the addition of NaOH, blue precipitates were formed immediately. The mixture was kept under stirring for more than 1 min, and then 25 mL of 0.10 M ascorbic acid solution was added into the mixture and stirred for another 15 min. Hereto, the uniform Cu_2O nanocubes with the size of 300-400 nm were fabricated. Then be centrifuged at 10000 rpm for 2 min; and after washed with water several times, and finally, dried under the condition of vacuum for the next experiments

1.2 Synthesis of Cu_7S_4 Hierarchical Hollow Cubic Cages Assembled by Ultrathin Nanosheets.

The obtained Cu_2O by the above procedure was added to 50 mL of water to make a suspension. Then 50 mL of 0.2 M thioacetamide (TAA) was added to this solution. After the addition of thioacetamide to the Cu_2O solution, the color changes from red to brown to black, gradually. The mixture was stirred at room temperature. After an additional 15 h of reaction under magnetic stirring; centrifuging at 6000 rpm for 5 min; and after several washings with water and ethanol, respectively; and finally, drying under the condition of vacuum, a black powder was obtained.

1.3 Synthesis of Cu_7S_4 Hierarchical Hollow Cubic Cages Assembled by ~20 nm Nanosheets.

The synthetic procedure was similar to that of the synthesis of Cu_7S_4 hierarchical hollow cubic cages assembled by ultrathin nanosheets except that the thioacetamide (TAA) was replaced by Na_2S.

1.4 Clock Reaction.

In a typical reaction, 50-300 μL (~1×10^{-5} M) of Cu_7S_4 nanocages was mixed with an aqueous solution of MB (200 μL of 5×10^{-4} M) in a 1 cm quartz cuvette, and the volume of the solution was made up to 3 mL. Next, 100 μL of 2.0 M aqueous hydrazine hydrate solution was added to the reaction mixture, and time-dependent absorption spectra were recorded in the UV-visible spectrophotometer at ~28 °C. The blue color of MB disappeared after 6.5 min. The solution regained its original blue shade just after (5-10 s) shaking in air. The visual dramatic reversible color change goes on for about 15 cycles. This might continue for a week when shaken for once or twice a day. Undisturbed solution remained colorless for days together.

1.5 Characterization.

Electronic absorption spectra of solid Cu_2O and Cu_7S_4 using diffuse reflectance spectra mode were recorded with a Cary model 5000 UV-vis/NIR spectrophotometer. Absorption spectra of the Cu_7S_4 nanocages solution were measured using a Shimadzu UV-2550 spectrometer. FT-IR spectral characteristics of the samples were collected with a Thermo-Fisher IS10 instrument. The phase and purity of the products Cu_2O and Cu_7S_4 were determined by X-ray powder diffraction (XRD) using an X-ray diffractometer with Cu Kα radiation (λ = 1.5418 Å). Scans were collected on dry nanomaterials in the range of 20-80°. The particle size, shape, and morphology of nanoparticles were observed with a field emission scanning electron microscope (Supra 40, Carl ZEISS Pvt. Ltd.), and an EDS machine (Oxford link and ISIS 300) attached to the instrument was used to obtain the nanocrystal composition. The structures of the samples were characterized using field-emission scanning microscopy (FE-SEM, Sirion200). TEM and HRTEM measurements of the metal oxide and sulfide sols were performed on a Hitachi H-9000 NAR instrument on samples prepared by placing a drop of fresh metal oxide and sulfide sols on copper grids precoated with carbon films, followed by solvent evaporation under vacuum. Atomic force microscopy (AFM) images of Cu_7S_4 nanosheets were recorded on a DI Innova. In the clock reaction, the time-dependent absorption spectra were recorded in the UV-visible spectrophotometer.

Acknowledgements

The authors would like to thank the National Natural Science Foundation of China (No. 51202253, 51002159).

Notes and references

[a] Institute of Intelligent Machines, Chinese Academy of Sciences, Hefei, Anhui, 230031, China. Email: zpzhang@iim.ac.cn, zywang@iim.ac.cn.
[b] Department of Chemistry, University of Science & Technology of China, Hefei, Anhui 230026, China.
[c] School of Physics and Engineering, Zhengzhou University, Zhengzhou, Henan, 450052, China.
† Y. C. Jiang and S. D. Zhang contributed equally to this work

Electronic Supplementary Information (ESI) available: XRD, EDS analysis, UV-Vis Spectra and additional material characterization. See DOI: 10.1039/b000000x/

1 (a) C. Wu, X. Lu, L. Peng, K. Xu, X. Peng, J. Huang, G. Yu, Y. Xie, *Nat. Commun.,* 2013, **4**, 2431; (b) M. Chhowalla, H. S. Shin, G. Eda, L.-J. Li, K. P. Loh, H. Zhang, *Nat. Chem.,* 2013, **5**, 263-275; (c) Y. Sun, Q. Liu, S. Gao, H. Cheng, F. Lei, Z. Sun, Y. Jiang, H. Su, S. Wei, Y. Xie, *Nat. Commun.,* 2013, **4**, 2899.

2 (a) X. D. Zhang, Y. Xie, *Chem. Soc. Rev.,* 2013, **42**, 8187-8199; (b).C. Wu, F. Feng, Y. Xie, *Chem. Soc. Rev.,* 2013, **42**, 5157-5183; (c) Y. Sun, S. Gao, Y. Xie, *Chem. Soc. Rev.,* 2014, **43**, 530-546; (d) Y. Sun, H. Cheng, S. Gao, Q. Liu, Z. Sun, C. Xiao, C. Wu, S. Wei, Y. Xie, *J. Am. Chem. Soc.,* 2012, **134**, 20294-20297; (e) X. Huang, Z. Zeng, H. Zhang, *Chem. Soc. Rev.,* 2013, **42**, 1934-1946.

3 (a) G. Zhang, B. Y. Xia, C. Xiao, L. Yu, X. Wang, Y. Xie, X W (David) Lou, *Angew. Chem. Int. Ed.,* 2013, **52**, 8643-8647; (b) C. Z. Yuan, J. Y Li, L. R. Hou, X. G. Zhang, L.F. Shen, X. W. (David) Lou, *Adv. Funct. Mater.,* 2012, **22**, 4592-4597. (c) J. B. Zhu, L. F. Bai, Y. F. Sun, X. D. Zhang, Q. Y. Li, B. X. Cao, W. S. Yan, Y. Xie, *Nanoscale*, 2013, **5**, 5241-5246; (d) J. Xie, H. Zhang, S. Li, R. Wang, X. Sun, M. Zhou, J. Zhou, X. W. (David) Lou, Y. Xie, *Adv. Mater.,* 2013, **25**, 5807-5813.

4 (a) G. Q. Zhang, X. W. (David) Lou, *Adv. Mater.*, 2013, **25**, 976-979; (b) Z. Y. Wang, X. W. (David) Lou, *Adv. Mater.,* 2012, **24**, 4124-4129; (c) A. Q. Pan, H. B. Wu, L.Yu, X. W. (David) Lou, *Angew. Chem.,* 2013, **125**, 2282-2286; (d) Z. Y. Wang, D. Y. Luan, F. Y. C. Boey, X. W. (David) Lou, *J. Am. Chem. Soc.,* 2011, **133**, 4738-4741.

5 (a) A. K. Geim, K. S. Novoselov, *Nat. Mater.,* 2007, **6**, 183-191; (b) Q. H. Wang, K. Kalantar-Zadeh, A. Kis, J. N. Coleman, M. S. Strano, *Nat. Nanotechnol.,* 2012, **7**, 699-712.

6 X. Zhang, J. Zhang, J. Zhao, B. Pan, M. Kong, J. Chen, Y. Xie, *J. Am. Chem. Soc.,* 2012, **134**, 11908-11911.

7 S. Z. Butler, S. M. Hollen, L. Cao, Y. Cui, J. A. Gupta, H. R. Gutie´rrez, T. F. Heinz, S. S. Hong, J. Huang, A. F. Ismach, E. Johnston-Halperin, M. Kuno, V. V. Plashnitsa, R. D. Robinson, R. S. Ruoff, S. Salahuddin, J. Shan, L. Shi, M. G. Spencer, M. Terrones, W. Windl, J. E. Goldberger, *ACS Nano,* 2013, **7**, 2898-2926.

8 (a) X. Zhang, X. Xie, H. Wang, J. Zhang, B. Pan, Y. Xie, *J. Am. Chem. Soc.,* 2013, **135**, 18-21; (b) J. Feng, X. Sun, C. Wu, L. Peng, C. Lin, S. Hu, J. Yang, Y. Xie, *J. Am. Chem. Soc.,* 2011, **133**, 17832-17838; (c) J. Feng, L. Peng, C. Wu, X. Sun, S. Hu, C. Lin, J. Dai, J. Yang, Y. Xie, *Adv. Mater.,* 2012, **24**, 1969-1974; (d) Y. Sun, H. Cheng, S. Gao, Z. Sun, Q. Liu, Q. Liu, F. Lei, T. Yao, J. He, S. Wei, Y. Xie, *Angew. Chem. Int. Ed.* 2012, **51**, 8727-8731; (e) L. Liu,

T. Yao, X. G. Tan, Q. H. Liu, Z. Q. Wang, D. C. Shen, Z. H. Sun, S. Q. Wei, Y. Xie, *Small,* 2012, **8**, 3752-3756.

9 (a) B. Radisavljevic, A. Radenovic, J. Brivio, V. Giacometti, A. Kis, *Nat. Nanotechnol.,* 2011, **6**, 147-150; (b) Z. Yin, H. Li, H. Li, L. Jiang, Y. Shi, Y. Sun, G. Lu, Q. Zhang, X. Chen, H. Zhang, *ACS Nano,* 2012, **6**, 74-80; (c) H. Li, G. Lu, Y. L. Wang, Z. Y. Yin, C. X. Cong, Q. Y. He, L Wang, F Ding, T Yu, H. Zhang, *Small,* 2013, **9**, 1974–1981; (d) Y. P. Du, Z. Y. Yin, J. X. Zhu, X. Huang, X. J. Wu, Z. Y. Zeng, Q. Y. Yan, H. Zhang, *Nat. Commun.,* 2012, **3**, 1177-1183; (e) Z. Y. Zeng, T. Sun, J. X. Zhu, X. Huang, Z. Y. Yin, G. Lu, Z. X. Fan, Q. Y. Yan, H. H. Hng, H. Zhang, *Angew. Chem. Int. Ed.,* 2012, **51**, 9052-9056.

10 J. N. Coleman, M. Lotya, A. O'Neill, S. D. Bergin, P. J. King, U. Khan, K. Young, A. Gaucher, S. De, R. J. Smith, I. V. Shvets, S. K. Arora, G. Stanton, H.-Y. Kim, K. Lee, G. T. Kim, G. S. Duesberg, T. Hallam, J. J. Boland, J. J. Wang, J. F. Donegan, J. C. Grunlan, G. Moriarty, A. Shmeliov, R. J. Nicholls, J. M. Perkins, E. M. Grieveson, K. Theuwissen, D. W. McComb, P. D. Nellist, V. Nicolosi, *Science,* 2011, **331**, 568-571.

11 K. S. Novoselov, D. Jiang, F. Schedin, T. J. Booth, V. V. Khotkevich, S. V. Morozov, A. K. Geim, *Proc. Natl. Acad. Sci. U. S. A.,* 2005, **102**, 10451-10453.

12 Y. H. Lee, X. Q. Zhang, W. Zhang, M. T. Chang, C. T. Lin, K. D. Chang, Y. C. Yu, J. T. W. Wang, C. S. Chang, L. J. Li, T. W. Lin, *Adv. Mater.,* 2012, **24**, 2320-2325.

13 K. K. Liu, W. Zhang, Y. H. Lee, Y. C. Lin, M. T. Chang, C. Y. Su, C. S. Chang, H. Li, Y. Shi, H. Zhang, C. S. Lai, L. J. Li, *Nano Lett.,* 2012, **12**, 1538-1544.

14 (a) D. A. Dikin, S. Stankovich, E. J. Zimney, R. D. Piner, G. H. Dommett, G. Evmenenko, S. T. Nguyen, R. S. Ruoff, *Nature,* 2007, **448**, 457-460; (b) L. Zhang, H. B. Wu, S. Madhavi, H. H. Hng, X. W. (David) Lou, *J. Am. Chem. Soc.,* 2012, **134**, 17388-17391; (c) B. Y. Xia, H. B. Wu, X. Wang, X. W. (David) Lou, *J. Am. Chem. Soc.,* 2012, **134**, 13934−13937.

15 (a) G. Eda, G. Fanchini, M. Chhowalla, *Nat. Nanotechnol.,* 2008, **3**, 270-274; (b) Z. Y. Wang, D. Y. Luan, F. Y. C. Boey, X. W. (David) Lou, *J. Am. Chem. Soc.,* 2011, **133**, 4738-4741.

16 (a) X. L. Li, G. Y. Zhang, X. D. Bai, X. M. Sun, X. R. Wang, E. G. Wang, H. J. Dai, *Nat. Nanotechnol.,* 2008, **3**, 538-542; (b) L. Zhang, H. Wu, X. W. (David) Lou, *J. Am. Chem. Soc.,* 2013, **135**, 10664-10672.

17 Z. P. Chen, W. C. Ren, L. B. Gao, B. L. Liu, S. F. Pei, H. M. Cheng, *Nat. Mater.,* 2011, **10**, 424-428.

18 F. Liu, T. S. Seo, *Adv. Funct Mater.,* 2010, **20**, 1930-1936.

19 Z. H. Tang, S. L. Shen, J. Zhuang, X. Wang, *Angew. Chem. Int. Ed.,* 2010, **49**, 4603-4607.

20 W. F. Chen, S. R. Li, C. H. Chen, L. F. Yan, *Adv. Mater.,* 2011, **23**, 5679-5683.

21 S. Stankovich, D. A. Dikin, G. H. B. Dommett, K. M. Kohlhaas, Z. E. J., E. A. Stach, R. Piner, S. T. Nguyen, R. S. Ruoff, *Nature,* 2006, **442**, 282-286.

22 T. Ramanathan, A. A. Abdala, S. Stankovich, D. A. Dikin, M. HERRERA-ALONSO, R. D. Piner, D. H. Adamson, H. C. Schniepp, X. Chen, R. S. Ruoff, S. T. Nguyen, I. A. Aksay, R. K. Prud'Homme, L. C. Brinson, *Nat. Nanotechnol.,* 2008, **3**, 327-331.

23 S. Ansari, A. Kelarakis, L. Estevez, E. P. Giannelis, *Small,* 2010, **6**, 205-209.

24 Y. Xu, K. Sheng, C. Li, G. Shi, *ACS Nano,* 2010, **4**, 4324-4330.

25 (a) S. D. Sun, X. P. Song, D. C. Deng, X. Z. Zhang, Z. M. Yang, *Catal. Sci. Technol.,* 2012, **2**, 1309-1314; (b) S. D. Sun, D. C. Deng, X. P. Song, Z. M. Yang, *Phys. Chem. Chem. Phys.,* 2013, **15**, 15964-15970.

26 (a) S. D. Sun, D. C. Deng, C. C. Kong, X. P. Song, Z. M. Yang, *Dalton Trans.,* 2012, **41**, 3214-3222; (b) S. D. Sun, X. P Song, C. C. Kong, D. C. Deng, Z. M. Yang, *CrystEngComm,* 2012, **14**, 67-70.

27 (a) S. D. Sun, S. Wang, D. C. Deng, Z. M. Yang, *New J. Chem.,* 2013, **37**, 3679-3684; (b) S. D. Sun, X. P. Song, C. C. Kong, S. H. Liang, B. J. Ding, Z. M. Yang, *CrystEngComm,* 2011, **13**, 6200-6205.

28 (a) S. H. Jiao, L. F. Xu, K. Jiang, D. S. Xu, *Adv. Mater.,* 2006, **18**, 1174-1178; (b) H. L. Cao, X. F. Qian, C. Wang, X. D. Ma, J. Yin, Z. K. Zhu, *J. Am. Chem. Soc.,* 2005, **127**, 16024-16025.

29 M. Behboudnia, B. Khanbabaee, *J. Cryst. Grow.* 2007, **304**, 158-162.

30 S. Pande, S. Jana, S. Basu, A. K. Sinha, A. Datta, T. Pal, *J. Phys. Chem. C,* 2008, **112**, 3619-3626.

31 G. Liu, X. Mu, H. Zhang P. Chen, *Chem. Sci.,* 2014, **5**, 275-280.

32 S. Basu, S. Panigrahi, S. Praharaj, S. K. Ghosh, S. Pande, S. Jana, A. Pal, T. Pal, *J. Phys. Chem. A,* 2007, **111**, 578-583.